The Astrophysical Journal, 897:172 (9pp), 2020 July 10 https://doi.org/10.3847/1538-4357/ab962a

Nonresonant Instability of Kinetic Alfvén Waves with κ-electrons

K. C. Barik[1], S. V. Singh, and G. S. Lakhina
Indian Institute of Geomagnetism Navi Mumbai, 410218, India; kcbarik17@gmail.com
Received 2020 March 13; revised 2020 May 1; accepted 2020 May 3; published 2020 July 15

Abstract

A nonresonant instability of kinetic Alfvén waves (KAWs) is studied in a three-component plasma system consisting of background cold ions, an ion beam, and hot electrons with a κ-distribution. The nonresonant KAW instability is produced by the combined sources of ion beam and velocity shear. It is found that the wave excitation by velocity shear alone will give rise to purely growing KAWs, whereas the ion beam velocity alone as a source cannot excite the waves for the considered plasma parameters. It is also observed that the combined sources of ion beam and velocity shear can excite the KAWs in nonresonant instability with finite wave frequency (the mode is not a purely growing mode). Also note that κ-electrons restrict the wave propagation very close to 90°, whereas the Maxwellian electrons permit the wave to propagate a few degrees away from 90°. It is inferred that the presence of κ-electrons shrinks the wave-unstable region of a KAW's nonresonant instability. The coupling between KAWs and ion-acoustic waves occurs at a lower value of β_i for Maxwellian electrons as compared to κ-electrons.

Unified Astronomy Thesaurus concepts: Solar wind (1534); Space plasmas (1544)

1. Introduction

The wave-particle interaction and the energy transfer mechanism from the tail side of the Earth's magnetosphere to the auroral ionosphere is a notable topic of interest in space physics. Many theories have been proposed to explain the energy transfer mechanism from the magnetosphere to the ionosphere. The kinetic Alfvén wave (KAW) is one of the agents responsible for transporting the energy from the distant magnetosphere to the auroral ionosphere (Louarn et al. 1994; Seyler et al. 1995; Chaston et al. 2005, 2006; Ergun et al. 2005; Artemyev et al. 2015; Gershman et al. 2017) due to the existence of a parallel component of a wave electric field along the ambient magnetic field direction (Thompson & Lysak 1996; Hui & Seyler 1992). The parallel electric field can be incorporated into the magnetohydrodynamic (MHD) waves for a small spatial scale, i.e., by making its perpendicular wavelength comparable to the ion gyroradius or electron inertial length. In the former situation, the wave is labeled as KAW and it requires that the electron thermal speed be larger than the Alfvén speed in the medium (Hasegawa & Chen 1976). This condition is usually satisfied in the magnetosphere above the altitude of 4–5R_E (Lysak & Carlson 1981), where R_E is the radius of Earth. In the latter situation, the wave is referred to as an inertial Alfvén wave, which exists when electron thermal speed is lower than the Alfvén speed of the medium (Goertz & Boswell 1979) and is observed in the Earth's magnetosphere below 4–5R_E (Lysak & Carlson 1981).

There are ample observational studies that support the existence of KAWs in various regions of Earth's magnetosphere, such as the magnetopause (Johnson et al. 2001; Chaston 2005), magnetosheath, auroral region (Boehm et al. 1990; Louarn et al. 1994; Wahlund et al. 1994), magnetotail, plasma sheet boundary layer (PSBL; Keiling et al. 2000, 2005; Keiling 2002; Wygant et al. 2002; Duan et al. 2012), and central plasma sheet (Keiling et al. 2001). The observational study by Wygant et al. (2002) showed that the increase in Poynting flux in the PSBL during the substorm expansion phase is related to the observation of KAWs. The turbulence observed in the solar wind is also attributed to the KAWs (Salem et al. 2012). From the THEMIS spacecraft observation, it is reported that in the spacecraft frame the fluctuations of the wave field in the frequency range of $f_{sc} \approx$ (0.2–20) Hz are well described by KAWs (Chaston et al. 2012). In a later study, ion heating in the plasma sheet by broadband KAWs was reported by Chaston et al. (2014). The energy exchange between the undamped KAWs and charged particles has been confirmed by Gershman et al. (2017) using Magnetosphere Multiscale mission data.

Like waves and instabilities such as MHD surface waves and Kelvin–Helmholtz instability, KAWs have been invoked to explain particle acceleration, anomalous transport, and ultra-low-frequency (ULF) waves in the Earth's magnetosphere (Angelo 1973, 1977; Chen & Hasegawa 1974; Hasegawa 1976; Hasegawa & Chen 1976; Hasegawa & Mima 1978; Goertz & Boswell 1979; Huba 1981; Lysak & Dum 1983; Lakhina 1987, 1990; Lysak & Lotko 1996; Thompson & Lysak 1996; Nosé et al. 1998). Theoretically, KAWs have been at the forefront of explaining the observed ULF waves. Lakhina (2008) studied the excitation of KAWs by velocity shear for resonant and nonresonant case for Maxwellian electrons. It was shown that the frequency of KAWs is in the range of ULF waves in the spacecraft frame. This study was further extended by Barik et al. (2019a, 2019b) to analyze the combined effect of ion beam and velocity shear on the excitation of KAWs. They showed that ion beam and velocity shear can act as a dual source that can excite the waves with a higher growth rate, compared to the single source of ion beam or velocity shear. Also, the anti-parallel ion beam streaming and positive velocity shear are found to be more favorable for the growth of KAWs. Observational evidence supports the particle distribution having a power-law distribution with a long energy tail. These distributions are best fit by a non-Maxwellian kappa distribution (Vasyliunas 1968; Livadiotis 2015; Lazar et al. 2016). Barik et al. (2019c) advanced one step further to study the instability produced in KAWs by velocity shear in the presence of kappa-distributed electrons for the resonant case.

The transition regions of Earth's magnetosphere, such as the magnetopause, magnetosheath, auroral region, polar cusp, magnetotail, PSBL, etc., are thick boundaries rather than thin

[1] Corresponding author.

through which the particle velocities change abruptly. These regions support a gradient in velocity that is called velocity shear and acts as a free energy source to excite waves. These velocity shears also change according to the background conditions. For example, during high solar activity due to high solar wind dynamic pressure, the compression of the magnetopause region increases, leading to an increase in the velocity shear. Also, during the expansion phase of the geomagnetic substorm, the compression of the magnetosphere from the night side further increases the velocity shear in the transition region. These were incorporated in our theoretical models presented earlier to see the effects of enhanced velocity shear on the growth rate of the KAWs. This analysis facilitates our understanding of various physical phenomena occurring in different magnetospheric regions, e.g., the increase in growth rate of KAWs due to increase in velocity shear can explain the enhanced Poynting flux in the PSBL during the substorm expansion phase (Wygant et al. 2002). The velocity shear along the field lines also acts as a free energy source for the generation of Kelvin–Helmholtz instability, which is responsible for the observed ULF waves in the polar cusp region (Angelo 1973, 1977).

Non-Maxwellian particle distributions and velocity shear have been observed in the solar wind and interplanetary medium. For example, Ulysses spacecraft observations (Schwadron 2002; McComas et al. 2003) reported the presence of transverse velocity shear in the solar wind created by latitudinal variation of velocity. Recently, Phan et al. (2020) reported that a substantial amount of transverse velocity shear is found in the solar wind using Parker Solar Probe (PSB) data during its first orbit. Hollweg et al. (2013) studied the velocity shear-induced mode coupling in the corona and solar wind. The effect of velocity shear on the fluctuating interplanetary magnetic field is studied by Jokipii et al. (2015). Also, non-Maxwellian electrons are observed in the solar wind (Jian et al. 2014). Gary et al. (2016) studied ion beam-driven instabilities in the solar wind using Wind spacecraft data. The expanding solar wind flow can lead to non-Maxwellian electron and ion velocity distributions, which can excite instabilities. These observational and theoretical studies revealed the existence of ion beam, velocity shear, and non-Maxwellian electrons in the solar wind and interplanetary medium. Motivated by these findings, we have developed a theoretical model that consists of Maxwellian background ions and beam ions and kappa-distributed electrons that can be applicable to Earth's magnetosphere and solar wind. The paper is arranged in the following manner. In Section 2 a theoretical model is presented. In Section 3 a generalized dispersion relation is derived for the combined case of ion beam and velocity shear. The nonresonant instability of KAWs driven by ion beam and velocity shear is discussed in Section 4. The numerical results are presented in Section 5. A discussion of the results and conclusions are presented in Section 6.

2. Theoretical Model

A three-component plasma model comprising Maxwellian background ions (N_i, T_i) and beam ions (N_B, T_B) and kappa-distributed electrons (N_e, T_e) is considered. Here, N_j and T_j are number density and temperature, respectively, which characterize the plasma species and $j = i$, e, and B for background ions, electrons, and beam ions respectively. The relation $N_e = N_i + N_B$ describes the quasi-neutrality condition in equilibrium. In this model, the background ions, although they have a finite temperature, are treated as cold species, and the electrons and beam ions are treated as hot species. Here, the cold species essentially refer to those that satisfy the condition $\frac{\omega^2}{k_\parallel^2 \alpha_i^2} \gg 1$, $\left(\alpha_i = \left(\frac{2T_e}{m_i}\right)^{1/2}\right)$, i.e., thermal speed of the background ions is small compared to the parallel phase velocity of the wave. Our analysis is based on kinetic theory, which takes into account all the forces through Vlasov's equation and Maxwell's equations. Livadiotis (2018) has shown the existence of two thermodynamic integrals characterizing the thermal equilibrium of a plasma system, the temperature and κ index. Therefore, the most general distribution function at thermal equilibrium is the kappa distribution, as in the limit of $\kappa \to \infty$, where one obtains a Maxwellian distribution. We assume the zeroth-order distribution function for the jth species to be a kappa distribution given by

$$f_{oj}(v_\perp, v_\parallel) = \pi^{-3/2}\frac{1}{\theta_j^3}\frac{\Gamma(\kappa+1)}{\kappa^{3/2}\Gamma(\kappa-1/2)}N_j \times \left(1 + \frac{v_\perp^2}{\kappa\theta_j^2} + \frac{(v_\parallel - V_j(X))^2}{\kappa\theta_j^2}\right)^{-(\kappa+1)}. \quad (1)$$

Here, Γ is the usual gamma function, and κ-index is a measure of non-Maxwellian characteristics; the smaller the κ value the more non-Maxwellian is the species, $v_\perp = \sqrt{v_x^2 + v_y^2}$ and $v_\parallel = v_z$, respectively, represents the perpendicular and parallel component of velocity with respect to the ambient magnetic field (i.e., z-direction), θ_j is the generalized thermal speed related to the normal thermal speed through the relation

$$\theta_j = \left[\left(\frac{\kappa - 3/2}{\kappa}\right)\right]^{1/2}\alpha_j = \left[\left(\frac{\kappa - 3/2}{\kappa}\right)\right]^{1/2}\left(\frac{2T_j}{m_j}\right)^{1/2} \quad (2)$$

where $\alpha_j = \left(\frac{2T_j}{m_j}\right)^{1/2}$ is the normal thermal speed. Here, $V_j(X)$ represents the non-uniform streaming of plasma species in the $z-$ direction, whereas it has a gradient in one of the directions perpendicular to the ambient magnetic field, i.e., the x-direction, where $X = x + v_y/\omega_{cj}$ is a constant of motion and $\omega_{cj} = \frac{q_j B_0}{cm_j}$ is the cyclotron frequency of plasma species, q_j and m_j are charge and mass of jth species, and c is the speed of light. Note that Equation (1) is valid for $\kappa > 3/2$. The zeroth-order Maxwellian distribution function for background ions and beam ions can be found from Equation (1) in the limit $\kappa \to \infty$.

Since we are assuming low beta plasma (i.e., the ratio of thermal pressure to magnetic pressure being much smaller than unity), the incompressibility of the magnetic field along the ambient magnetic field direction allows us to write the wave electric field as the gradient of two different scalar potential (Hasegawa 1976), i.e., ψ, along the parallel direction and ϕ, along the perpendicular direction

$$\boldsymbol{E} = -\nabla_\perp\phi + E_\parallel\hat{z} = -\nabla_\perp\phi - \nabla_\parallel\psi. \quad (3)$$

The first-order distribution (perturbed distribution) function can be derived by solving the linearized Vlasov's equation. This is achieved by assuming the perturbation to be of the form $\sim\exp(ik_\perp y + ik_\parallel z - i\omega t)$, where $k_\perp$ and $k_\parallel$ are the perpendicular and parallel components of propagation vector $\boldsymbol{k}$,

respectively, with respect to the ambient magnetic field, and ω is the frequency of KAWs. We have also assumed a local approximation of $L_v k \gg 1$ to solve the Vlasov's equation, where $L_v = V_j/(dV_j/dx)$ is the velocity gradient scale length and $k = \sqrt{k_y^2 + k_z^2}$ is the wavenumber. The final form of the perturbed distribution function is given by Lakhina (2008) and Barik et al. (2019a, 2019b, 2019c) as

$$f_{1j} = \frac{e_j}{m_j}\sum_{n=-\infty}^{+\infty}\sum_{m=-\infty}^{+\infty}\frac{e^{i(n-m)\theta}}{(k_\parallel v_z - \omega + n\omega_{cj})} \times J_n(\xi_j)J_m(\xi_j) \times (k_\perp M_j\phi + k_\parallel L_j\psi), \quad (4)$$

where

$$M_j = \left(1 - \frac{k_\parallel v_z}{\omega}\right)\left[\frac{\partial f_{0j}}{\partial v_\perp}\cdot\frac{n\omega_{cj}}{k_\perp v_\perp} + \frac{1}{\omega_{cj}}\cdot\frac{\partial f_{0j}}{\partial x}\right] + \frac{\partial f_{0j}}{\partial v_z}\frac{n\omega_{cj}}{\omega}\frac{k_\parallel}{k_\perp}, \quad (5)$$

$$L_j = \frac{k_\perp v_z}{\omega}\left[\frac{\partial f_{0j}}{\partial v_\perp}\cdot\frac{n\omega_{cj}}{k_\perp v_\perp} + \frac{1}{\omega_{cj}}\cdot\frac{\partial f_{0j}}{\partial x}\right] + \left(1 - \frac{n\omega_{cj}}{\omega}\right)\frac{\partial f_{0j}}{\partial v_z}. \quad (6)$$

Here, a cylindrical coordinate system is used to derive this relation, i.e., $\boldsymbol{v} = (v_\perp, \theta, v_\parallel)$, where θ is the angle the velocity vector makes with the ambient magnetic field, and $J_n(\xi_j)$ and $J_m(\xi_j)$ are the Bessel function of orders n and m, respectively, with argument $\xi_j = \left(\frac{k_\perp v_\perp}{\omega_{cj}}\right)$.

The perturbed number density and parallel current density can be derived from Equation (4) using the relations

$$n_j = \int d^3v f_{1j}, \quad J_{zj} = \int d^3v e_j v_z f_{1j}. \quad (7)$$

The perturbed number and current density for the background ions and beam ions can be derived from Equation (7) using the Maxwellian distribution function as the zeroth-order distribution and are exactly the same as Equations (10) and (11) of Barik et al. (2019a) and that for the non-Maxwellian electrons can be obtained using the κ distribution as the zeroth-order distribution and are the same as Equations (16) and (17) of Barik et al. (2019c).

The number density n_j and parallel (z-component) current density J_{zj} are used in Poisson's equation and the z-component of Ampere's law to derive the dispersion relation and are given by:

(Poisson's equation)

$$-\nabla_\perp^2\phi + \frac{\partial E_\parallel}{\partial z} = 4\pi\sum_j e_j n_j; \quad (8)$$

(the z-component of Ampere's law)

$$\frac{\partial\nabla_\perp^2\phi}{\partial z} + \nabla_\perp^2 E_\parallel = \frac{4\pi}{c^2}\frac{\partial}{\partial t}\sum_j J_{zj} \quad (9)$$

Keeping in mind that the KAWs are the low-frequency electromagnetic waves (i.e., $\omega \ll \omega_{cj}$) and assuming nearly perpendicular propagation of the waves (i.e., $k_\parallel \ll k_\perp$), Equations (8) and (9) can be written as

$$\begin{bmatrix} D_{11} & D_{12} \\ D_{21} & D_{22}\end{bmatrix}\begin{bmatrix}\phi \\ \psi\end{bmatrix} = 0. \quad (10)$$

The coefficients are given by

$$D_{11} = k_\perp^2\left[1 + \left(\frac{\kappa - 1}{\kappa}\right)^{1/2}\left\{\frac{\omega_{pe}^2}{\omega_{ce}^2}\right\} + \sum_l\frac{2\omega_{pl}^2}{k_\perp^2\alpha_l^2}\frac{\bar\omega}{\omega}(1 - b_l)\right], \quad (11)$$

$$D_{12} = k_\parallel^2\left[1 + \frac{\omega_{pe}^2}{k_\parallel^2\theta_e^2}\left\{\frac{(2\kappa - 1)}{\kappa} + \frac{i\sqrt{\pi}\,\kappa!}{\kappa^{3/2}\Gamma(\kappa - 1/2)}\left(\frac{2\omega}{k_\parallel\theta_e}\right)\right\} - \sum_l\frac{\omega_{pl}^2 b_l}{k_\parallel^2\alpha_l^2}Z'\left(\frac{\bar\omega}{k_\parallel\alpha_l}\right)\left(1 - S_l\frac{k_\perp}{k_\parallel}\right)\right], \quad (12)$$

$$D_{21} = k_\parallel k_\perp^2\left[1 + \sum_l\frac{\omega_{pl}^2 b_l}{c^2k_\perp^2}S_l\frac{k_\perp}{k_\parallel}\right] \quad (13)$$

$$D_{22} = -k_\parallel k_\perp^2\left[1 - \frac{\omega_{pe}^2}{c^2k_\perp^2}\left\{\frac{(2\kappa - 1)}{\kappa}\frac{\omega^2}{k_\parallel^2\theta_e^2} + \frac{i\sqrt{\pi}\,\kappa!}{\kappa^{3/2}\Gamma(\kappa - 1/2)}\frac{2\omega^3}{k_\parallel^3\theta_e^3}\right\} + \sum_l\frac{\omega_{pl}^2}{c^2k_\perp^2}\left\{\frac{b_l\omega^2}{k_\parallel^2\alpha_l^2}Z'\left(\frac{\bar\omega}{k_\parallel\alpha_l}\right)\left(1 - S_l\frac{k_\perp}{k_\parallel}\right) + S_l\frac{k_\perp}{k_\parallel}\right\}\right], \quad (14)$$

where, $\omega_{pe} = \left(\frac{4\pi N_e e^2}{m_e}\right)^{1/2}$ is the electron plasma frequency, $\omega_{pl} = \left(\frac{4\pi N_l e^2}{m_l}\right)^{1/2}$ is the plasma frequency of lth species, where $l = i$ and B for background ions and beam ions, respectively, $\bar\omega = (\omega - k_\parallel V_l)$ is the Doppler-shifted frequency of lth species, $S_l = \left(\frac{1}{\omega_{cl}}\right)\left(\frac{dV_l}{dx}\right)$ and $\alpha_l = \left(\frac{2T_l}{m_l}\right)^{1/2}$ are the velocity shear and thermal speed of lth species, respectively, $b_l = I_0(\lambda_l)\exp(-\lambda_l)$, $I_0(\lambda_l)$ is the zeroth-order modified Bessel function, $\lambda_l = k_\perp^2\alpha_l^2/2\omega_{cl}^2$, and $Z'(\frac{\bar\omega}{k_\parallel\alpha_l})$ is the derivative of the plasma dispersion function. Note that while arriving at the coefficients Equations (11)–(14), it is assumed that the electrons have no drift and velocity shear, i.e., $V_e = 0 = S_e$, thus the absence of a shear term in the expressions of electrons.

3. Generalized Dispersion Relation

The generalized dispersion relation is obtained by following the procedures of Lakhina (2008) and Barik et al. (2019a). This is achieved by assuming the beam ions have drifting velocity V_B and velocity shear $S_B = S$, and background ions without drift and velocity shear, i.e., $V_i = 0$ and $S_i = 0$. Under the assumptions, $\frac{\omega^2}{k_\parallel^2\alpha_i^2} \gg 1$, $\frac{\omega^2}{k_\parallel^2\alpha_e^2} \ll 1$, $\lambda_e < 1$, and $\frac{\omega^2}{k_\parallel^2\alpha_B^2} \leqslant 1$, the general dispersion relation is obtained by equating the

determinant of Equation (10) and is given by

$$\frac{b_i N_i}{N_e}\left[1 + a_1 - \frac{\omega^2}{k_\parallel^2 v_A^2}\frac{N_i}{N_e}\frac{1-b_i}{\lambda_i}Aq_0\right] - \frac{\omega^2}{k_\parallel^2 c_s^2}\left[C_R' + i(1+a_1)C_I - \frac{\omega^2}{k_\parallel^2 v_A^2}\frac{N_i}{N_e}\frac{1-b_i}{\lambda_i}A(C_R + iC_I)\right] = \frac{2\omega^2}{k_\parallel^2 \alpha_i^2}\frac{(1-b_i)N_i}{N_e}, \quad (15)$$

where

$$a_1 = \frac{N_B}{N_e}\frac{\beta_B b_B}{2\lambda_B} S\frac{k_\perp}{k_\parallel}, \quad (16)$$

$$q_0 = 1 + \frac{N_B}{N_i}\frac{m_i}{m_B}\frac{S k_\perp}{b_i k_\parallel}, \quad (17)$$

$$A = 1 + \frac{N_B}{N_i}\frac{T_i}{T_B}\frac{\bar{\omega}}{\omega}\frac{(1-b_B)}{(1-b_i)}, \quad (18)$$

$$C_R = \frac{(2\kappa-1)}{(2\kappa-3)} + \frac{N_B}{N_e}\frac{T_e}{T_B} b_B\left(1 - S\frac{k_\perp}{k_\parallel}\right), \quad (19)$$

$$C_R' = \frac{(2\kappa-1)}{(2\kappa-3)} + \frac{N_B}{N_e}\frac{T_e}{T_B} \times \left\{b_B\left(1 - \frac{\bar{\omega}}{\omega}\right) + \left(\frac{\bar{\omega}}{\omega} - b_B S\frac{k_\perp}{k_\parallel}\right)\right\} + a_1 C_R, \quad (20)$$

$$C_I = \sqrt{\pi}\frac{\omega}{k_\parallel \theta_e}\left[\frac{\kappa!}{\kappa^{3/2}\Gamma(\kappa-1/2)}\frac{2\kappa}{(2\kappa-3)} + b_B\frac{N_B}{N_e}\left(\frac{T_e}{T_B}\right)^{3/2}\left(\frac{m_B}{m_e}\right)^{1/2}\frac{\bar{\omega}}{\omega}\left(1 - S\frac{k_\perp}{k_\parallel}\right)\left(\frac{2\kappa-3}{2\kappa}\right)^{1/2}\exp\left(-\frac{\bar{\omega}^2}{k_\parallel^2 \alpha_B^2}\right)\right]. \quad (21)$$

Here, $v_A = \frac{B_0}{\sqrt{4\pi N_e m_i}}$ is the Alfvén speed, and $\bar{\omega} = (\omega - k_\parallel V_B)$ $\beta_i = (8\pi N_e T_i/B_0^2)$ and $\beta_B = (8\pi N_e T_B/B_0^2)$ are the ion and beam plasma betas, respectively. Note that in multi-component plasmas, ion-acoustic speed can be defined by taking into account the temperatures and densities of the constituent's, as has been done in Dubinov & Senilov (2011), Saberian (2019), and several other papers, e.g., Moolla et al. (2010). However, for ease of numerical computations and to study the effect of variation of different constituent's temperatures and densities on the dispersion characteristics of the waves, we have defined the ion-acoustic speed in terms of electron temperature and background ions (protons) mass as $c_s = \left(\frac{T_e}{m_i}\right)^{1/2}$. Though one can also take the approach discussed in abovementioned papers. Here, C_I represents the damping due to electrons and beam ions.

By neglecting the damping term and in the absence of beam ions, i.e., $N_B = 0$, Equation (15) is reduced to

$$\left[b_i - \frac{(2\kappa-1)}{(2\kappa-3)}\frac{\omega^2}{k_\parallel^2 c_s^2}\right]\cdot\left[1 - \frac{\omega^2}{k_\parallel^2 v_A^2}\frac{(1-b_i)}{\lambda_i}\right] = \frac{2\omega^2(1-b_i)}{k_\parallel^2 \alpha_i^2}, \quad (22)$$

which is the same as Equation (26) of Barik et al. 2019c. It shows the coupling between ion-acoustic waves (IAWs) and KAWs in the presence of a kappa electron and reduces to the same expression as Equation (36) of Hasegawa & Chen (1976) and Equation (23) of Lakhina (2008) in the limit $\kappa \to \infty$. In the smaller plasma beta limit, i.e., $\beta_i \ll 1$, the coupling between these two waves becomes weak and the modes get decoupled, as shown in Equations (27) and (28) of Barik et al. (2019c) and the limit $\kappa \to \infty$ reduces to Equations (24) and (25) of Lakhina (2008).

4. Nonresonant Instability of KAWs

In this section, we study the nonresonant instability of KAWs. When the thermal speed of the plasma species is comparable to the phase velocity of the wave, resonance occurs in the system and this kind of instability is known as resonant instability. However, there are situations when the contribution from the resonant particles is negligible, and the wave still grows because of the free energy supplied by the nonresonant particle distributions. This type of instability is called nonresonant instability. The electrostatic two-stream instability is a well-known example of a nonresonant instability (Nicholson 1983; Lakhina 1994). From Equation (15), neglecting the C_I term, the contribution from the imaginary part that gives rise to the growth/damping of the wave in resonant instability vanishes and we are left with only the real part of the equation. If the solution of the real part gives one of the roots as imaginary, that will contribute to the growth/damping of the wave in nonresonant instability. However, roots can also be purely imaginary or a combination of real and imaginary parts. The former will be considered a purely growing mode. It is worth mentioning here that the growth/damping term arises in the system for the resonant case that is studied by the kinetic approach only. Nonresonant instabilities can be studied by neglecting growth/damping terms and also be described by a fluid kind of picture. Furthermore, wave-particle interactions can be studied by resonant instability, whereas they cannot be studied by nonresonant instability. Here, nonresonant instability is studied by solving the following simplified equation, which is obtained from Equation (15) by putting $C_I = 0$:

$$\frac{\omega^4}{k_\parallel^4 v_A^4}\left[\frac{N_i}{N_e}\frac{(1-b_i)}{\lambda_i}AC_R\right] - g_1\frac{\omega^2}{k_\parallel^2 v_A^2} + \frac{N_i}{N_e}\frac{b_i\beta_i}{2}(1+a_1) = 0. \quad (23)$$

The solution of the equation Equation (23) can be written as

$$\omega^2 = \frac{k_\parallel^2 v_A^2}{2}\frac{\lambda_i N_e}{(1-b_i)AN_i C_R}[g_1 \pm (g_1^2 - 4g_0)^{1/2}], \quad (24)$$

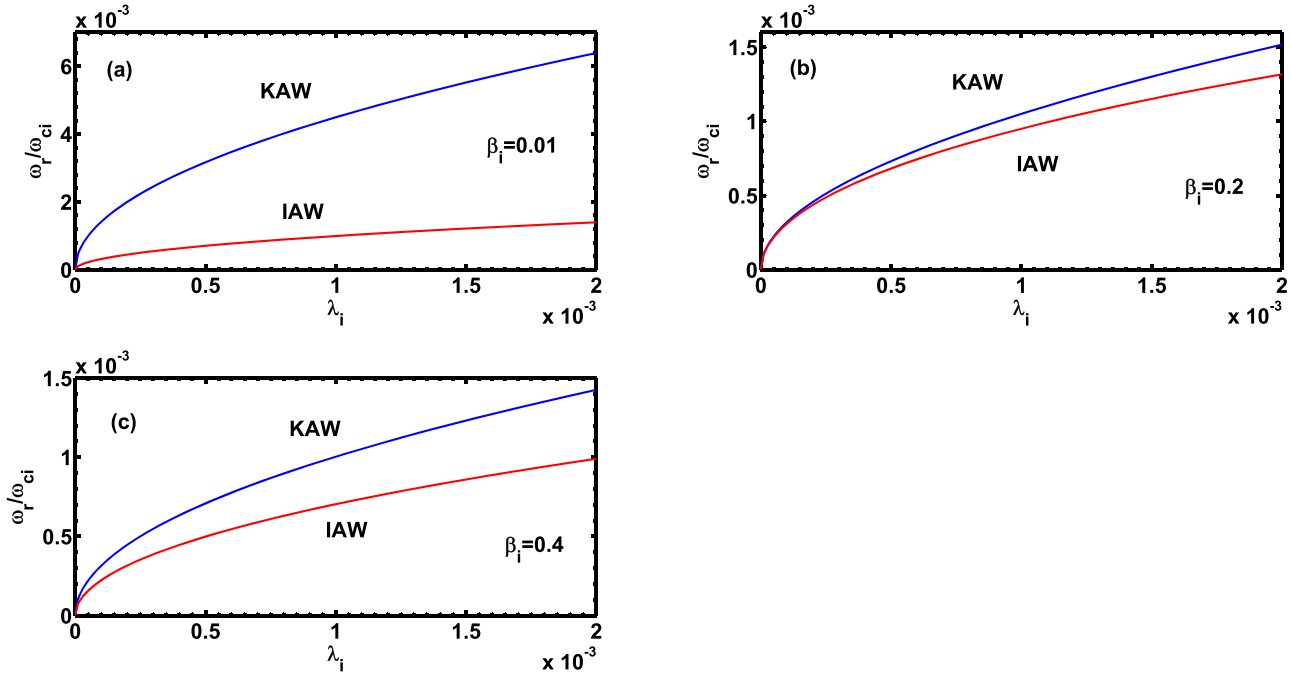

Figure 1. Coupling of KAWs and IAWs in the presence of Maxwellian electrons for plasma parameters, $T_i/T_e = 0.1$, $k_\parallel/k_\perp = 0.01$, $\kappa = \infty$ and for different values of $\beta_i = 0.01$ for (a), 0.2 for (b), and 0.4 for (c), respectively, as mentioned on the curves.

where

$$g_0 = \left(\frac{N_i}{N_e}\right)^2 \frac{b_i\beta_i}{2}\frac{(1-b_i)}{\lambda_i}(1+a_1)AC_R, \tag{25}$$

$$g_1 = \left[C_R' + \frac{N_i}{N_e}(1-b_i)\left\{\frac{T_e}{T_i} + \frac{N_i}{N_e}\frac{b_i\beta_i}{2\lambda_i}Aq_0\right\}\right]. \tag{26}$$

The nonresonant instability is obtained when $C_R < 0$ and from this a threshold condition for the velocity shear is found to be

$$S_{\rm th} = \frac{k_\parallel}{k_\perp}\left[1 + \frac{(2\kappa-1)}{(2\kappa-3)}\frac{N_e}{N_B}\frac{T_B}{b_B T_e}\right] \tag{27}$$

In the limit $\kappa \to \infty$, the above expression reduces to Equation (32) of Lakhina (2008). It is apparent from Equation (27) that larger velocity shear is required to excite nonresonant instabilities with non-Maxwellian electrons, compared to Maxwellian electrons.

5. Numerical Analysis

It is well known that in the low β limit, the coupling between KAWs and IAWs will become weak and these two waves will decouple. We examine the decoupling of KAWs and IAWs in the presence of non-Maxwellian κ-electrons ($\kappa = 2$) and compare with the case of Maxwellian electrons ($\kappa = \infty$) for the set of plasma parameters, $T_i/T_e = 0.1$, $k_\parallel/k_\perp = 0.01$, and for different β_i. The coupled dispersion relation Equation (22) is solved numerically and the two positive roots are plotted to show the coupling and decoupling of KAWs and IAWs. For Maxwellian electrons, Figure 1 delineates three different phases: (a) the decoupled KAW (blue curve) and IAW (red curve), (b) the starting phase of coupling, and (c) the coupling of KAW and IAW at a larger β_i. It can be seen that at smaller β_i (=0.01 for the parameters considered here), two distinct decoupled modes, i.e., the KAW and IAW are observed, which remain decoupled up to $\beta_i < 0.2$. The coupling of the two modes starts at $\beta_i \approx 0.2$ (Figure 1(b)) and continues to couple at higher values of β_i (Figure 1(c)). Note that with increasing β_i, the coupling occurs at lower values of λ_i. Figure 2 describes the coupling and decoupling of KAWs and IAWs for non-Maxwellian κ-electrons. Although the same trend continues, i.e., at smaller values of β_i the two waves remain decoupled and get coupled at larger β_i values, it is quite interesting that for κ-electrons, the coupling starts at a comparatively higher value of β_i (=0.6 here) and also at a lower value of wave frequency as compared to the Maxwellian electrons. This is due to the fact that κ-electron lowers the wave frequency.

The critical value of β_i obtained from our computations is important for the coupling and decoupling of the KAWs and IAWs. For β_i values smaller than the critical value, the KAWs and IAWs remain as two independent decoupled modes. At the critical value of β_i, the coupling between the two modes starts and continues for higher values of β_i. Once the coupling starts, it is difficult to distinguish between KAWs and IAWs. There is theoretical evidence that supports the decoupling of KAWs and IAWs (Hasegawa & Chen 1976; Lakhina 2008; Barik et al. 2019c), although numerically it is not shown. Though we are not aware of observations showing coupling between KAWs and IAWs, our analysis predicts that for β_i greater than the critical values, the observed low-frequency electromagnetic modes would not be purely KAWs but will also have some properties of IAWs.

Now, we numerically evaluate growth rate of nonresonant instability of the KAWs in non-Maxwellian plasmas. The typical plasma parameters considered for the computations are $N_B/N_e = 0.5$, $S = 0.5$, $\beta_i = 0.01$, $k_\parallel/k_\perp = 0.005$, $\kappa = 2, 4, 6, \infty$. The normalized growth rate obtained from Equation (24) is plotted for different variations in the plasma parameters. We have used similar normalizations as adopted by Lakhina (2008)

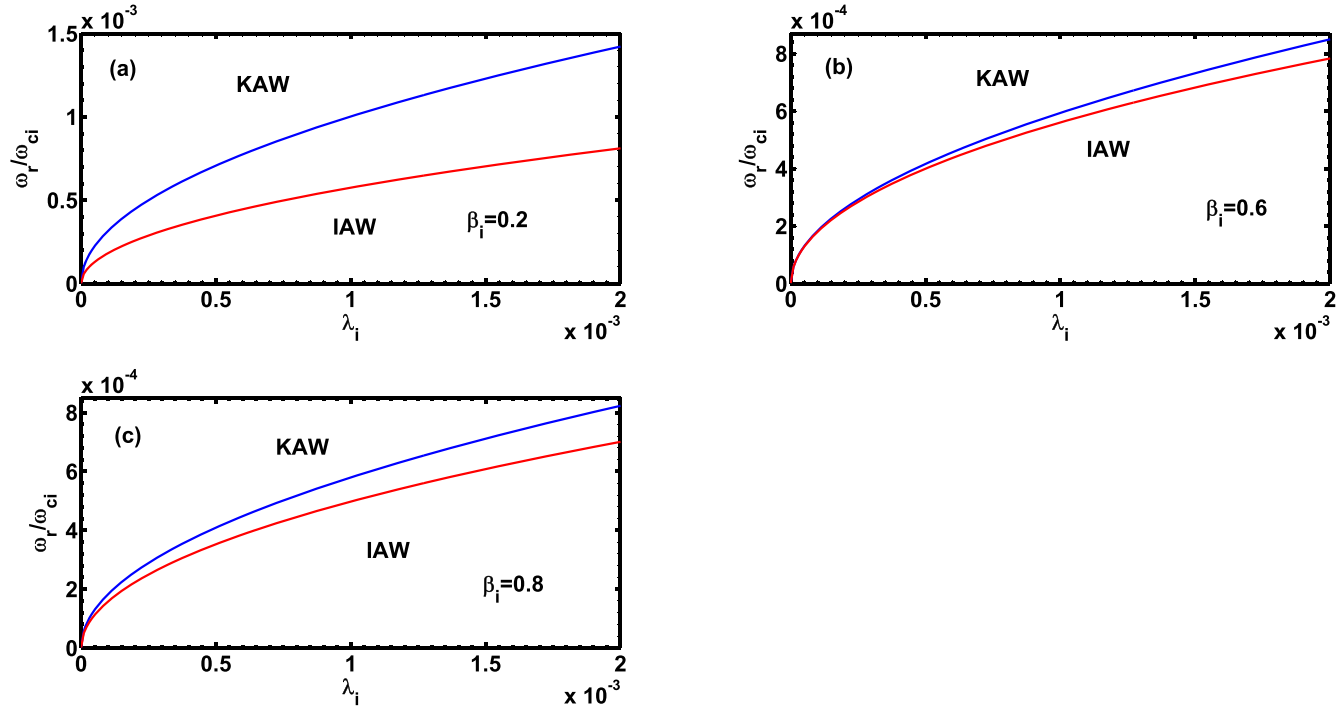

Figure 2. Coupling of KAWs and IAWs in the presence of κ-electrons for plasma parameters, $T_i/T_e = 0.1$, $k_\parallel/k_\perp = 0.01$, $\kappa = 2$ and for different values of $\beta_i = 0.2$ for (a), 0.6 for (b), and 0.8 for (c), respectively, as mentioned on the curves.

and Barik et al. (2019a), i.e., frequencies ω_r are normalized with respect to ion beam cyclotron frequency ω_{cB}, temperatures with ion beam temperature T_B, and streaming velocity V_B, with thermal speed of ion beam, α_B.

Figure 3 delineates variation of growth rates of KAWs with the square of normalized perpendicular wavenumber, $\lambda_B = \frac{k_\perp^2 \alpha_B^2}{2\omega_{cB}^2}$, for various values of κ-index and other plasma parameters described in the previous paragraph. The growth rate of nonresonant instability increases with a decrease in κ index at a fixed value of λ_B and the growth rate is at maximum for highly non-Maxwellian electrons (smaller κ). Note that with decreasing κ value, the wave-unstable region (i.e., the range of λ_B for which the growth rate of the KAW's nonresonant instability is obtained) also decreases. Similar results are found in the resonant KAW instability (Barik et al. 2019c), thus it can be inferred that the presence of non-Maxwellian electrons narrows down the wave-unstable region in both nonresonant and resonant KAW instabilities.

Figure 4 shows the dependence of the growth rate of nonresonant instability on velocity shear for $\kappa = 2$ and ∞. The other plasma parameters are the same as those in Figure 3. The peak growth rate and the unstable region (in wavenumbers) of the instability increases with increasing velocity shear. For comparison, we have also plotted the growth rate for $\kappa = \infty$ and S = 0.2. It is obvious from the curves that non-Maxwellian electrons restrict the unstable region and at small wavenumbers the growth rate is higher for non-Maxwellian electrons than the Maxwellian electrons. The peak growth rate shifts toward larger wavenumbers with increasing velocity shear. For all values of velocity shear shown here, the growth rate initially increases slowly and then rises sharply as λ_B is increased. The peak growth rate is higher for Maxwellian electrons, compared to the non-Maxwellian electrons for the same value of velocity shear.

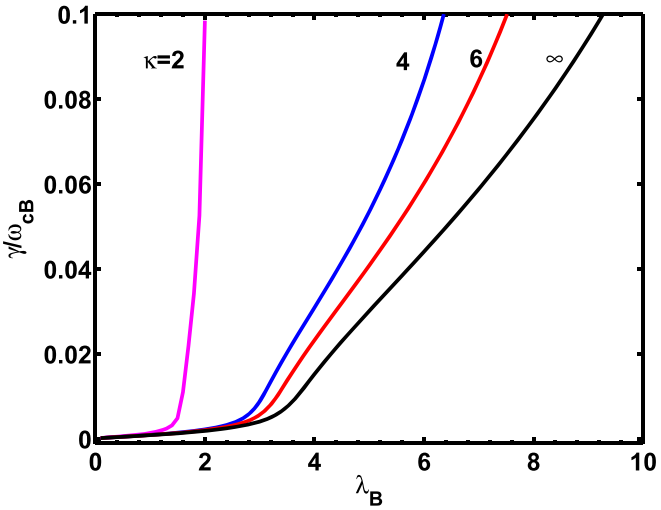

Figure 3. KAW nonresonant instability showing variation of normalized growth rate vs. $\lambda_B = \frac{k_\perp^2 \alpha_B^2}{2\omega_{cB}^2}$ for $N_B/N_e = 0.5$, $S = 0.5$, $\beta_i = 0.01$, $k_\parallel/k_\perp = 0.005$, and for various values of κ, as mentioned on the curves.

Numerically, we find that the threshold of velocity shear is inversely related with the non-Maxwellian index κ, i.e., the lower the non-Maxwellian index (i.e., more non-Maxwellian electrons), the higher the velocity shear threshold value to excite nonresonant KAWs. From our computations, it is found that the threshold velocity shear $S_{\rm th} = 0.18$, 0.1, and 0.07 for electrons with $\kappa = 2$, 3, and for Maxwellian electrons ($\kappa = \infty$), respectively. The effect of ion beam velocity on the growth rate of nonresonant KAW instability is also tested. It is found that the ion beam alone is unable to excite the nonresonant KAW instability for the plasma parameters considered here. The combined effect of ion beam and velocity shear on the excitation of KAWs is also examined. It is

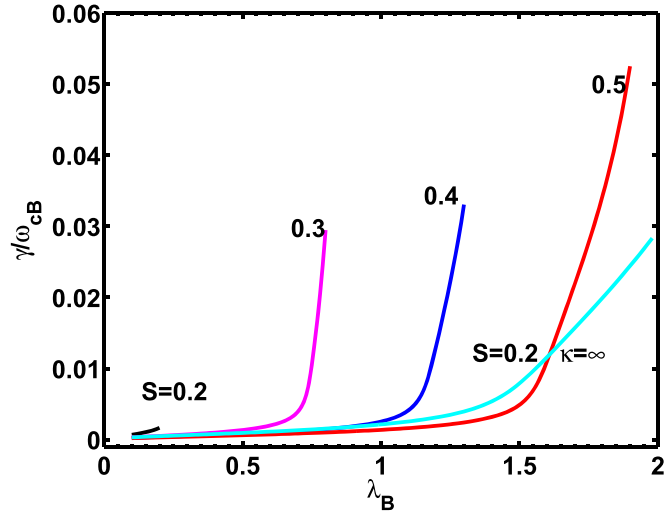

Figure 4. KAW nonresonant instability showing variation of normalized growth rate vs. $\lambda_B = \frac{k_\perp^2 \alpha_B^2}{2\omega_{cB}^2}$ for $N_B/N_e = 0.5$, $\kappa = (2, \infty)$, $\beta_i = 0.01$, $k_\parallel/k_\perp = 0.005$, and for various values of velocity shear S, as mentioned on the curves.

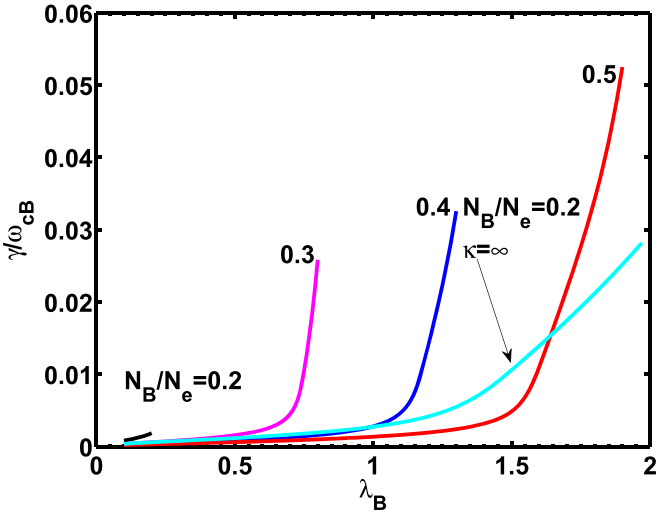

Figure 5. KAW nonresonant instability showing variation of normalized growth rate vs. $\lambda_B = \frac{k_\perp^2 \alpha_B^2}{2\omega_{cB}^2}$ for $S = 0.5$, $\kappa = (2, \infty)$, $\beta_i = 0.01$, $k_\parallel/k_\perp = 0.005$, and for various values of number density N_B/N_e, as mentioned on the curves.

observed that in the presence of a finite positive velocity shear and ion beam velocity, the growth rate of the KAWs is not affected significantly but now the wave mode is not a purely growing mode. Note that the nonresonant KAW instability excited by the velocity shear alone is a purely growing mode. However, the inclusion of ion beam velocity introduces a finite real frequency to the nonresonant KAW instability.

The effect of variation of ion beam number density on the growth rate of KAWs for non-Maxwellian ($\kappa = 2$) and Maxwellian ($\kappa = \infty$) electrons is depicted in Figure 5. It can be seen that for the non-Maxwellian electrons with increasing number density N_B/N_e, the peak growth rate increases and a spread in the λ_B range is noticed. For the same value of number density ($N_B/N_e = 0.2$ here), the peak growth rate and the range of unstable wavenumbers of KAWs is larger for Maxwellian electrons compared to non-Maxwellian electrons. It is observed that similar to velocity shear, the critical value of number density is reciprocally related to non-Maxwellian index κ. Our computation confirms that a critical number density of 0.17 is required for a non-Maxwellian electron ($\kappa = 2$); the critical value should be 0.10 for electrons with $\kappa = 3$, and for a Maxwellian electron, a critical value of 0.06 is required to excite the waves.

Figure 6 shows the variation of growth rate of KAWs with λ_B for different values of $k_\parallel/k_\perp$ for non-Maxwellian and Maxwellian electrons. The other plasma parameters are the same as those in Figure 3. It is seen that with decreasing $k_\parallel/k_\perp$ (increase in angle of propagation) the unstable region shifts toward a higher λ_B region. The peak growth rate occurs at larger values of λ_B for subsequent increases in angle of propagation. From our computations it is found that for nonresonant instability of KAWs, no growth is obtained for $k_\parallel/k_\perp \geqslant 0.015$ ($\theta = 89.^\circ14$) for non-Maxwellian electrons with $\kappa = 2$, $k_\parallel/k_\perp \geqslant 0.026$ ($\theta = 88.^\circ51$) for $\kappa = 3$, $k_\parallel/k_\perp \geqslant 0.031$ ($\theta = 88.^\circ22$) for $\kappa = 4$ and $k_\parallel/k_\perp \geqslant 0.042$ ($\theta = 87.^\circ59$) for Maxwellian electrons. Hence, it can be inferred that Maxwellian electrons allow the waves to propagate a few degrees away from 90°, whereas kappa electrons restrict the wave propagation very close to 90° for nonresonant instability of KAWs.

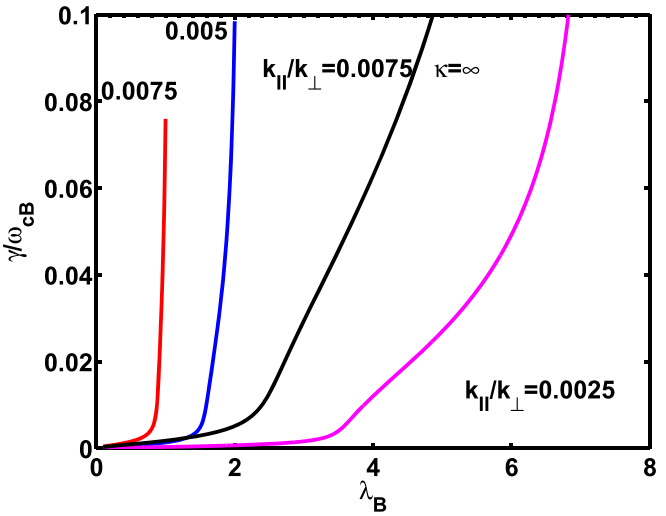

Figure 6. KAW nonresonant instability showing variation of normalized growth rate vs. $\lambda_B = \frac{k_\perp^2 \alpha_B^2}{2\omega_{cB}^2}$ for $S = 0.5$, $\kappa = (2, \infty)$, $\beta_i = 0.01$, $N_B/N_e = 0.5$, and for various values of propagation angle $k_\parallel/k_\perp$, as mentioned on the curves.

Figure 7 illustrates the variation of KAW growth rates with λ_B for non-Maxwellian and Maxwellian electrons for different T_e/T_B ratios. For non-Maxwellian electrons($\kappa = 2$) peak growth rates are shifted to higher λ_B values with increasing T_e/T_B and waves are excited for a higher λ_B range. Although not shown here, the effect of β_i on the excitation of nonresonant KAWs instability with kappa electrons is examined. It is found that changes in β_i have a marginal effect on the excitation of nonresonant KAWs.

6. Discussion and Conclusion

We have studied KAWs in three-component plasma consisting of kappa electrons, protons, and ion beam. First, coupling and decoupling of IAWs and KAWs is examined in a plasma with κ-electrons and protons. It is shown that the decoupling of IAWs and KAWs occurs at a higher value of ion plasma β_i and lower-wave frequency in the presence of

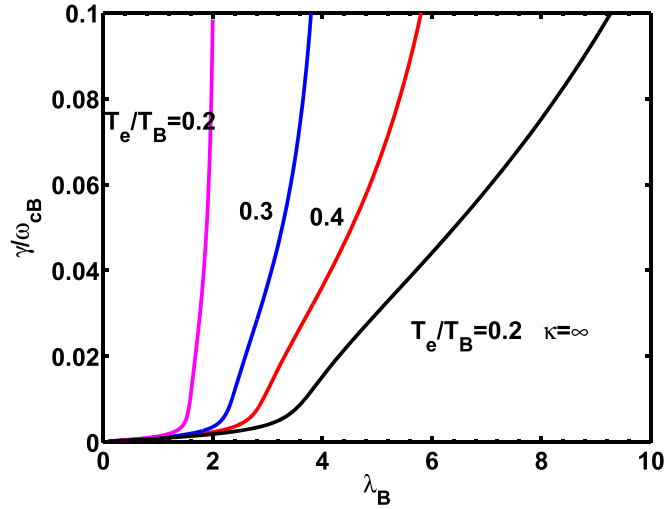

Figure 7. KAW nonresonant instability showing variation of normalized growth rate vs. $\lambda_B = \frac{k_\perp^2 \alpha_B^2}{2\omega_{cB}^2}$ for $S = 0.5$, $\kappa = (2, \infty)$, $\beta_i = 0.01$, $k_\parallel/k_\perp = 0.005$, $N_B/N_e = 0.5$, and for various values of temperature ratio T_e/T_B, as mentioned on the curves.

non-Maxwellian electrons as compared to the Maxwellian one. Furthermore, a nonresonant instability of KAWs generated by ion beam and velocity shear has been discussed. It is found that non-Maxwellian electrons restrict the unstable region of KAWs in the wavenumber regime, but tend to increase the growth rate of the instability. It is observed that for the plasma parameters considered here, an ion beam as a single free energy source cannot excite the nonresonant KAW instability, whereas velocity shear alone can excite the purely growing KAWs. On the other hand, when ion beam and velocity shear are simultaneously present, KAWs with finite real frequency are generated with a substantial growth rate. The threshold velocity shear is inversely related to the non-Maxwellian index κ, i.e., for highly non-Maxwellian electrons a large velocity shear is required to excite nonresonant KAWs and vice versa.

The critical value of ion beam number density is reciprocally related to the non-Maxwellian κ-index. A large peak growth rate for KAWs is obtained for propagation angle close to 90° for non-Maxwellian electrons and for the same propagation angle a larger peak growth is found for Maxwellian electrons compared to the κ electrons. Note that for non-Maxwellian electrons the wave propagation is restricted only very close to 90°, whereas it is permissible for few degrees away from 90° for Maxwellian electrons. The growth rate of the nonresonant KAW instability peaks at a larger value of wavenumber when the temperature of the non-Maxwellian electrons increases. At the same electron temperature, the Maxwellian electrons tend to enhance the wave-unstable region. The ion plasma β_i has a marginal effect on the growth of KAWs in nonresonant instability.

It is found that the features of nonresonant instability of KAWs are similar to the resonant case studied by Barik et al. (2019c). In resonant instability the wave propagation is allowed up to $\theta \leqslant 82°$ ($\theta \leqslant 76.^\circ 50$) for non-Maxwellian (Maxwellian) electrons, whereas in nonresonant instability this range is $\theta \leqslant 89.^\circ 14$ ($\theta \leqslant 87.^\circ 59$). Thus, the nonresonant instability is limited to a highly oblique propagation angle. In both cases the critical value of the ion beam number density and the threshold of velocity shear increases with decreasing κ-index, i.e., a high critical ion beam number density and a large velocity shear are required to excite KAWs with non-Maxwellian electrons, compared to Maxwellian electrons. In both cases, the increase in non-Maxwellian electron (i.e., low κ index) temperature tends to increase the wave-unstable region of KAWs. On the other hand, the magnitude of the growth rate for nonresonant instability is much larger than that for the resonant case. The perpendicular and parallel wavelengths range are quite high in the nonresonant case compared to the resonant one.

For application purposes, we have taken the plasma parameters relevant to the auroral/polar cusp region at an altitude of 5–7R_E, where R_E represents Earth's radius (Lysak & Lotko 1996; Lakhina 2008; Barik et al. 2019a). The available parameters are ion beam densities, $N_B/N_e = (0.01–0.2)$, $V_B/\alpha_B < 2$, where we assume $N_B/N_e = (0.1–0.5)$, $\beta_i = (0.001–1.0)$ and $S = (0.01–0.5)$. Also, we consider the ion beam cyclotron frequency, $\omega_{cB}/2\pi \approx$ (2.2–3.0) Hz common at the auroral altitude of 5–7R_E, the hot electron temperature, $T_e \approx 100$ eV, the background cold ion temperature, $T_i \approx 10$ eV, and the beam ion temperature, $T_B \approx$ 1–2 keV.

The maximum normalized growth rate (Figure 4) is found to be 0.053 at $\lambda_B = 1.9$, whereas this is excited in the λ_B range of (0.1–1.9). The corresponding un-normalized growth rate is obtained as 0.1325 Hz. The un-normalized growth rate falls in the range of (0.5–132.5) mHz for the whole range of our computation. The perpendicular wavenumber can be calculated from the relation $k_\perp = \sqrt{2\lambda_B}\,\omega_{cB}/\alpha_B$ and is found as (0.01–0.05) km^{-1} and the corresponding perpendicular wavelength is (628 − 125) km. The parallel wavenumber can be found from the relation $k_\parallel/k_\perp = 0.005$ and is given by (0.05–0.25) × 10^{-3} km^{-1} and the respective parallel wavelength is (125 − 25)×10^3 km.

The perpendicular wavelength of (125–628) km obtained for the KAW from our model matches the upper value of the observed wavelengths of (20–120) km in the polar region (Wygant et al. 2002). The above model may be able to explain some of the observed characteristics of ULF waves in the Earth's magnetosphere.

Although we have presented an application of the model to the auroral region of Earth's magnetosphere, it can also be applied to other regions of the magnetosphere, solar wind, and the interplanetary medium, where signatures of ion beam, velocity shear, and non-Maxwellian electrons are evident.

G.S.L. thanks the Indian National Science Academy, New Delhi for the support under INSA-Honorary Scientist Scheme.

ORCID iDs

K. C. Barik https://orcid.org/0000-0003-3958-4587
S. V. Singh https://orcid.org/0000-0003-2758-7713
G. S. Lakhina https://orcid.org/0000-0002-8956-486X

References

Angelo, N. D. 1973, JGR, 78, 1206
Angelo, N. D. 1977, RvGeo, 15, 299
Artemyev, A. V., Rankin, R., & Blanco, M. 2015, JGRA, 120, 305
Barik, K. C., Singh, S. V., & Lakhina, G. S. 2019a, PhPl, 26, 022901
Barik, K. C., Singh, S. V., & Lakhina, G. S. 2019b, URSI Radio Science Bulletin, 26, 17
Barik, K. C., Singh, S. V., & Lakhina, G. S. 2019c, PhPl, 26, 112108
Boehm, M. H., Carlson, C. W., McFadden, J. P., Clemmons, J. H., & Mozer, F. S. 1990, JGR, 95, 12157

Chaston, C. C., Bonnell, J. W., Clausen, L., & Angelopoulos, V. 2012, JGRA, 117, A12205
Chaston, C. C., Bonnell, J. W., & Salem, C. 2014, GeoRL, 41, 8185
Chaston, C. C., Genot, V., Bonnell, J. W., et al. 2006, JGRA, 111, A03206
Chaston, C. C., Phan, T. D., Bonnell, J. W., et al. 2005, PhRvL, 95, 065002
Chaston, C. C. 2005, JGRA, 110, A02211
Chen, L., & Hasegawa, A. 1974, JGR, 79, 1024
Duan, S., Liu, Z., & Angelopoulos, V. 2012, ChSBu, 57, 1429
Dubinov, A. E., & Senilov, L. A. 2011, TePhL, 37, 900
Ergun, R. E., Andersson, L., Su, Y.-J., et al. 2005, PhPl, 12, 072901
Gary, S. P., Jian, L. K., Broiles, T. W., et al. 2016, JGRA, 121, 30
Gershman, D. J., F-Vinas, A., Dorelli, J. C., et al. 2017, NatCo, 8, 14719
Goertz, C. K., & Boswell, R. W. 1979, JGR, 84, 7239
Hasegawa, A. 1976, JGR, 81, 5083
Hasegawa, A., & Chen, L. 1976, PhFl, 19, 1924
Hasegawa, A., & Mima, K. 1978, JGR, 83, 1117
Hollweg, J. V., Kaghashvili, E. K., & Chandran, B. D. G. 2013, ApJ, 769, 142
Huba, J. D. 1981, JGR, 86, 8991
Hui, C. H., & Seyler, C. E. 1992, JGR, 97, 3953
Jian, L. K., Wei, H. Y., Russell, C. T., et al. 2014, ApJ, 786, 123
Johnson, J. R., Cheng, C. Z., & Song, P. 2001, GeoRL, 28, 227
Jokipii, J. R., Kóta, J., & Giacalone, J. 2015, JPhCS, 577, 012015
Keiling, A. 2002, JGRA, 107, 1132
Keiling, A., Parks, G. K., Wygant, J. R., et al. 2005, JGRA, 110, A10S11
Keiling, A., Wygant, J. R., Cattell, C., et al. 2000, GeoRL, 27, 3169
Keiling, A., Wygant, J. R., Cattell, C., et al. 2001, JGR, 106, 5779
Lakhina, G. 2008, AdSpR, 41, 1688
Lakhina, G. S. 1987, JGR, 92, 12161
Lakhina, G. S. 1990, Ap&SS, 165, 153
Lakhina, G. S. 1994, PhyS, T50, 114
Lazar, M., Fichtner, H., & Yoon, P. H. 2016, A&A, 589, A39
Livadiotis, G. 2015, JGRA, 120, 880
Livadiotis, G. 2018, EL, 122, 50001
Louarn, P., Wahlund, J. E., Chust, T., et al. 1994, GeoRL, 21, 1847
Lysak, R. L., & Carlson, C. W. 1981, GeoRL, 8, 269
Lysak, R. L., & Dum, C. T. 1983, JGR, 88, 365
Lysak, R. L., & Lotko, W. 1996, JGR, 101, 5085
McComas, D. J., Elliott, H. A., Schwadron, N. A., et al. 2003, GeoRL, 30, 1517
Moolla, S., Bharuthram, R., Singh, S. V., Lakhina, G. S., & Reddy, R. V. 2010, PhPl, 17, 022903
Nicholson, D. R. 1983, Introduction to Plasma Theory (New York: Wiley)
Nosé, M., Iyemori, T., Sugiura, M., et al. 1998, JGR, 103, 17587
Phan, T. D., Bale, S. D., Eastwood, J. P., et al. 2020, ApJS, 246, 34
Saberian, E. 2019, ApJ, 887, 121
Salem, C. S., Howes, G. G., Sundkvist, D., et al. 2012, ApJ, 745, L9
Schwadron, N. A. 2002, GeoRL, 29, 1663
Seyler, C. E., Wahlund, J.-E., & Holback, B. 1995, JGR, 100, 21453
Thompson, B. J., & Lysak, R. L. 1996, JGR, 101, 5359
Vasyliunas, V. M. 1968, JGR, 73, 7519
Wahlund, J.-E., Louarn, P., Chust, T., et al. 1994, GeoRL, 21, 1831
Wygant, J. R., Keiling, A., Cattell, C. A., et al. 2002, JGRA, 107, 1201